Photonic band structures solved by a plane-wave-based transfer-matrix method

Zhi-Yuan Li and Lan-Lan Lin
Ames Laboratory and Department of Physics and Astronomy, Iowa State University, Ames, Iowa 50011
(Received 20 November 2002; revised manuscript received 21 January 2003; published 15 April 2003)

Transfer-matrix methods adopting a plane-wave basis have been routinely used to calculate the scattering of electromagnetic waves by general multilayer gratings and photonic crystal slabs. In this paper we show that this technique, when combined with Bloch's theorem, can be extended to solve the photonic band structure for 2D and 3D photonic crystal structures. Three different eigensolution schemes to solve the traditional band diagrams along high-symmetry lines in the first Brillouin zone of the crystal are discussed. Optimal rules for the Fourier expansion over the dielectric function and electromagnetic fields with discontinuities occurring at the boundary of different material domains have been employed to accelerate the convergence of numerical computation. Application of this method to an important class of 3D layer-by-layer photonic crystals reveals the superior convergency of this different approach over the conventional plane-wave expansion method.

DOI: 10.1103/PhysRevE.67.046607 PACS number(s): 42.70.Qs, 42.50.Dv, 32.80.−t

I. INTRODUCTION

Photonic crystals, a novel class of material where the refractive index is periodic in space, have stimulated extensive interest of study in recent years. Characterized by photonic band structures and photonic band gaps, these materials can mold the flow of photons much like conventional semiconductors do to electrons. Armed with unprecedented power to control the light propagation behavior through a variety of optical functional elements such as waveguides, cavities, bends, and branches in sizes comparable to the wavelength of light, photonic crystals can serve as the platform for future integrated optical circuits [1–3].

A basic while important tool to understand the characteristic of a photonic crystal is the photonic band structure, which represents the dispersion of photons (called Bloch's photons) with respect to their propagation directions and polarization states. A frequency range in the photonic band structure within which no photons exist irrespective of the direction and polarization is called a complete photonic band gap. Numerous theoretical approaches have been developed in literatures to calculate the photonic band structure for two-dimensional (2D) and three-dimensional (3D) photonic crystals. These include conventional plane-wave expansion method (PWM) [4–6], real-space transfer-matrix method (TMM) [7,8], finite-difference time-domain method [9], and Korringa-Kohn-Rostoker (KKR) method [10–14] for systems built from spherical or cylindrical particles. Different from the conventional PWM, the real-space TMM [7,8] and the KKR methods [11,12,14] look upon the photonic crystal as an infinite stack of identical periodic crystal layers along a certain direction, and thus an infinitely thick grating. Correspondingly, Maxwell's equations are solved within every single layer, and electromagnetic (em) fields among different layers are connected to each other through a transfer matrix. Recently, within the general framework of transfer-matrix formulation, various approaches have been exploited with different types of basis functions used to represent the em fields, including the Rayleigh multipoles [14], analytical modal functions [15], and Fourier modal functions (also called plane-wave functions) [15–20]. In addition to solution of photonic band structures, the TMM can also handle the wave scattering by a photonic crystal slab, leading to the transmission and reflection spectra, quantities directly observed experimentally, an advantage over the more popular conventional PWM.

In this paper, we will investigate in detail the plane-wave based TMM and apply this approach to calculate the photonic band structures for 2D and 3D photonic crystals with arbitrary lattice types and unit cell configurations. Three different numerical schemes to solve the eigenproblem leading to traditional band diagrams [plotted along the high-symmetry lines of the first Brillouin zone (BZ)] will be proposed and discussed. Comparison will be made between the current method and the conventional PWM regarding the numerical convergency. This paper is arranged as follows. In Sec. II and Appendixes A and B, we give a brief description of the plane-wave based TMM in application to wave scattering by 2D and 3D photonic crystal slabs, and corresponding eigenproblem connected with the photonic band structure. Two different eigenproblem schemes are discussed. In Sec. III, we will illustrate how to construct the traditional band diagrams by looking at different layer stacking directions for 2D and 3D photonic crystals. In Sec. IV we consider a 3D layer-by-layer photonic crystal to show how to build the whole band diagram by only looking at one single stacking direction. In Sec. V we further discuss third eigenproblem scheme, which combines the merits of the first two schemes. In Sec. VI we conclude this paper.

II. PLANE-WAVE-BASED TMM FOR WAVE SCATTERING AND PHOTONIC BAND STRUCTURE SOLUTIONS

In a general wave scattering problem, we suppose a plane em wave is incident from the left-hand side on a photonic crystal slab placed in an air background. Let the wave propagate along the z-axis direction, the incident wave vector is $\mathbf{k}_0=(k_{0x},k_{0y},k_{0z})$. For the present, we consider a general three-dimensional (3D) photonic crystal slab, corresponding to which we are dealing with the scattering problem of em

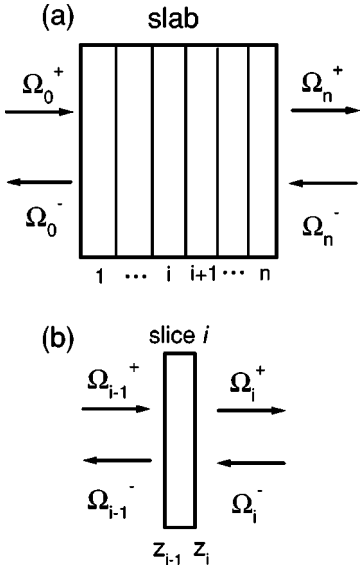

FIG. 1. (a) Definition of the *S* matrix in the transfer-matrix method for a photonic crystal slab, which is divided into a number of thin slices. (b) Definition of the *S* matrix for an individual slice.

waves by a 2D grating. The situation of a 2D photonic crystal slab (and thus the scattering problem of a 1D grating) can be directly derived from the 3D case. See Appendixes A and B. Let the primitive lattice $\mathbf{R}$ of the grating in the XY plane has two unit vectors $\mathbf{a}_1$ and $\mathbf{a}_2$, and the corresponding reciprocal lattice $\mathbf{G}$ has two unit vectors of $\mathbf{b}_1$ and $\mathbf{b}_2$.

The em fields at an arbitrary point $\mathbf{r}$ can be written into the superposition of Bragg waves (or plane waves):

$$\mathbf{E}(\mathbf{r})=\sum_{ij}\ \mathbf{E}_{ij}(z)e^{i(k_{ij,x}x+k_{ij,y}y)}, \tag{1}$$

$$\mathbf{H}(\mathbf{r})=\sum_{ij}\ \mathbf{H}_{ij}(z)e^{i(k_{ij,x}x+k_{ij,y}y)}, \tag{2}$$

where the Bragg wave vector $\mathbf{k}_{ij}=(k_{ij,x},k_{ij,y})=(k_{0x},k_{0y})+i\mathbf{b}_1+j\mathbf{b}_2$, $\mathbf{E}_{ij}$, and $\mathbf{H}_{ij}$ are unknown expansion coefficients of the electric and magnetic fields. In principle, the indices i and j should run from $-\infty$ to $+\infty$, but in numerical practice, truncation over a certain order is necessary. To solve the unknown variables $\mathbf{E}_{ij}$ and $\mathbf{H}_{ij}$, the whole photonic crystal slab is divided into a number of thin slices, as shown in Fig. 1(a), where each slice can be approximated as a lamellar 2D grating, within which the dielectric function is constant along the *z*-axis direction. If the slab has already been a lamellar grating, no division procedure is required. We further imagine that each slice (indexed from 1,2, . . . , to n) is surrounded by an infinitely thin film of air in both hand sides. This amounts to place the whole diffraction problem into a plane-wave basis in the air background. With a zero thickness, these artificial air thin films will generate no impact to the diffraction problem.

As shown in Fig. 1(b), the em fields in the two air thin films around the ith slice is both consisting of forwards and backwards propagating plane waves. The tangential components of the electric field in the left hand-side air film can be written into

$$E_{x(y)}(\mathbf{r})=\sum_{ij}\ [E^+_{ij,x(y)}(z)+E^-_{ij,x(y)}(z)]e^{ik_{ij,x}x+ik_{ij,y}y}, \tag{3}$$

where $E^+_{ij,x(y)}(z)=E^+_{ij,x(y)}e^{i\beta_{ij}(z-z_{i-1})}=E^+_{ij,x(y)}$, $E^-_{ij,x(y)}(z)=E^-_{ij,x(y)}e^{-i\beta_{ij}(z-z_{i-1})}=E^-_{ij,x(y)}$, since $z=z_{i-1}$. β_{ij} is given by $\beta_{ij}=(k_0^2-k_{ij,x}^2-k_{ij,y}^2)^{1/2}$ for $k_0^2-k_{ij,x}^2-k_{ij,y}^2\geqslant 0$, and $\beta_{ij}=i(k_{ij,x}^2+k_{ij,y}^2-k_0^2)^{1/2}$ for $k_0^2-k_{ij,x}^2-k_{ij,y}^2<0$. The tangential components of the magnetic field are

$$H_{x(y)}(\mathbf{r})=\sum_{ij}\ [H^+_{ij,x(y)}(z)+H^-_{ij,x(y)}(z)]e^{ik_{ij,x}x+ik_{ij,y}y}, \tag{4}$$

where $H^+_{ij,x(y)}(z)=H^+_{ij,x(y)}e^{i\beta_{ij}(z-z_{i-1})}=H^+_{ij,x(y)}$, $H^-_{ij,x(y)}(z)=H^-_{ij,x(y)}e^{-i\beta_{ij}(z-z_{i-1})}=H^-_{ij,x(y)}$. For each Bragg wave vector we have the following relation between the $\mathbf{H}$ and $\mathbf{E}$ fields: $(H^+_{ij,x},H^+_{ij,y})^T=T_{0,ij}(E^+_{ij,x},E^+_{ij,y})^T$, and $(H^-_{ij,x},H^-_{ij,y})^T=-T_{0,ij}(E^-_{ij,x},E^-_{ij,y})^T$, where the superscript "T" denotes matrix transposition. The 2×2 matrix $T_{0,ij}$ has matrix elements $T^{11}_{0,ij}=-k_{ij,x}k_{ij,y}/(k_0\beta_{ij})$, $T^{12}_{0,ij}=(k^2_{ij,x}-k_0^2)/(k_0\beta_{ij})$, $T^{21}_{0,ij}=(k_0^2-k^2_{ij,y})/(k_0\beta_{ij})$, and $T^{22}_{0,ij}=k_{ij,x}k_{ij,y}/(k_0\beta_{ij})$. The em fields in the right-hand side air film have the same form of expansion. In Eqs. (3) and (4) we simply replace $E^\pm_{ij,x(y)}$ and $H^\pm_{ij,x(y)}$ with $U^\pm_{ij,x(y)}$ and $V^\pm_{ij,x(y)}$, respectively. $V^\pm_{ij,x(y)}$ and $U^\pm_{ij,x(y)}$ are also connected to each other through the 2×2 matrix $T_{0,ij}$.

Having written down the em fields around the slice, we need to further solve the em fields inside the 2D lamellar grating slice. The procedure has been described in Appendixes A and B. By defining column vectors $\Omega^\pm_{i-1}=(\cdots,E^\pm_{ij,x},E^\pm_{ij,y},\cdots)^T$, $\Omega^\pm_i=(\cdots,U^\pm_{ij,x},U^\pm_{ij,y},\cdots)^T$, where $-N\leqslant i\leqslant N$, $-M\leqslant j\leqslant M$, with N and M being the truncation orders, we have

$$\begin{pmatrix}\Omega_i^+\\ \Omega_i^-\end{pmatrix}=T_i\begin{pmatrix}\Omega_{i-1}^+\\ \Omega_{i-1}^-\end{pmatrix}. \tag{5}$$

T_i is called the transfer matrix (more accurately, the T-matrix) for the ith slice. The overall T matrix for the whole slab is simply given by $T=T_nT_{n-1}\cdots T_i\cdots T_2T_1$, a simple multiplication. Although simple in nature, this T-matrix method proves to be numerically unstable for thick gratings such as the photonic crystal slabs studied here. The reason is that the evanescent wave components in the plane-wave expansion will increase exponentially when the T matrices for all slices accumulate, as can be found in Appendix A. One scheme to overcome this numerical instability is the scattering-matrix (S-matrix) method [7,8,20]. In this method, the transfer matrix for the ith slice in Eq. (5) is redefined as

$$\begin{pmatrix}\Omega_i^+\\ \Omega_{i-1}^-\end{pmatrix}=s^i\begin{pmatrix}\Omega_{i-1}^+\\ \Omega_i^-\end{pmatrix}. \tag{6}$$

s^i is called the *S* matrix for slice *i*. The overall *S* matrix of the whole slab *S* is connected to individual s_i through a simple iteration algorithm [7,8,20]. When the overall *S* matrix is solved, one can easily obtain the transmission and reflection coefficients for the grating slab under arbitrary incidence conditions.

With the layer transfer matrix at hand, we can directly solve the photonic band structure. Assume the primitive lattice vectors of a 3D photonic crystal are $\mathbf{a}_1$, $\mathbf{a}_2$, and $\mathbf{a}_3$. Note that these three vectors are not necessarily orthogonal to each other for a general lattice, say, a face-centered cubic (fcc) or face-centered tetragonal (fct) lattice. We can always set the plane formed by $\mathbf{a}_1$ and $\mathbf{a}_2$ as the *XOY* plane, which means that in this plane we have a 2D lattice with primitive lattice vectors $\mathbf{a}_1$ and $\mathbf{a}_2$. The corresponding reciprocal lattice vectors are $\mathbf{b}_1=2\pi(\mathbf{a}_2\times\hat{\mathbf{z}})/[(\mathbf{a}_1\times\mathbf{a}_2)\cdot\hat{\mathbf{z}}]$, $\mathbf{b}_2=2\pi(\hat{\mathbf{z}}\times\mathbf{a}_1)/[(\mathbf{a}_1\times\mathbf{a}_2)\cdot\hat{\mathbf{z}}]$, and a general reciprocal vector is given by $\mathbf{G}_{ij}=i\mathbf{b}_1+j\mathbf{b}_2$. The whole infinite photonic crystal is looked upon as an infinite number of layers stacking along the *z*-axis direction, every layer having the same primitive lattice vectors ($\mathbf{a}_1$ and $\mathbf{a}_2$) and reciprocal lattice vectors ($\mathbf{b}_1$ and $\mathbf{b}_2$).

The key to jump from a general wave scattering problem to a photonic band structure problem is to impose a periodic boundary condition along the stacking direction of the infinite grating. According to Bloch's theorem, the field at $\mathbf{r}$ is connected to the field at $\mathbf{r}+\mathbf{R}$ through $u(\mathbf{r}+\mathbf{R})=e^{i\mathbf{k}\cdot\mathbf{R}}u(\mathbf{r})$, where *u* is one of the components of either *E* field or *H* field, $\mathbf{k}=(k_x,k_y,k_z)$ is the Bloch's wave vector, and $\mathbf{R}$ is a lattice vector of the 3D lattice. The periodic boundary condition along the *z*-axis direction leads to

$$u(\mathbf{r}+\mathbf{a}_3)=e^{i\mathbf{k}\cdot\mathbf{a}_3}u(\mathbf{r}). \tag{7}$$

Thus we need to work out the transfer matrix connecting the field at $\mathbf{r}$ and $\mathbf{r}+\mathbf{a}_3$. Remember that in Eqs. (5) and (6) the transfer matrix is strictly propagating along the stacking direction, namely, the *z* axis. Thus, after we get the transfer matrix connecting $u(x,y,z_0)$ and $u(x,y,z_0+a_{3,z})$, we should further phase shift $u(x,y,z_0+a_{3,z})$ to $u(x+a_{3,x},y+a_{3,y},z_0+a_{3,z})$. Observing that $u(x,y,z_0+a_{3,z})=\Sigma u_{ij}(z_0+a_{3,z})\exp[ik_{ij,x}x+ik_{ij,y}y]$, and $u(x+a_{3,x},y+a_{3,y},z_0+a_{3,z})=\Sigma u_{ij}(z_0+a_{3,z})\exp[ik_{ij,x}a_{3,x}+ik_{ij,y}a_{3,y}]\exp[ik_{ij,x}x+ik_{ij,y}y]$, we can easily find out the transformation rule of both the *T* matrix and *S* matrix under this phase shift. Another important point is that in application of the transfer-matrix technique, the Bragg wave vectors for the 2D lattice in the *XOY* plane should take $(k_{ij,x},k_{ij,y})=(k_x+G_{ij,x},k_y+G_{ij,y})$.

After the transfer matrix connecting $u(\mathbf{r}+\mathbf{a}_3)$ and $u(\mathbf{r})$ is finally settled down, we are ready to move forward to solve the photonic band structure. Denoting the column vector of the fields in the both hand sides of the primitive unit cell as (Ω_1^+,Ω_1^-) and (Ω_0^+,Ω_0^-), in the *T*-matrix algorithm we write

$$\begin{pmatrix}\Omega_1^+\\ \Omega_1^-\end{pmatrix}=T\begin{pmatrix}\Omega_0^+\\ \Omega_0^-\end{pmatrix}. \tag{8}$$

From Bloch's theorem Eq. (7), we have $\Omega_1^+=e^{i\mathbf{k}\cdot\mathbf{a}_3}\Omega_0^+$ and $\Omega_1^-=e^{i\mathbf{k}\cdot\mathbf{a}_3}\Omega_0^-$. Then Eq. (8) becomes

$$T\begin{pmatrix}\Omega_0^+\\ \Omega_0^-\end{pmatrix}=e^{i\mathbf{k}\cdot\mathbf{a}_3}\begin{pmatrix}\Omega_0^+\\ \Omega_0^-\end{pmatrix}, \tag{9}$$

which means that Bloch's phase factor is the eigenvalue of the *T* matrix for a unit cell of the photonic crystal layer. To appreciate numerical stability, we need to turn to the *S*-matrix algorithm. From equation

$$\begin{pmatrix}\Omega_1^+\\ \Omega_0^-\end{pmatrix}=S\begin{pmatrix}\Omega_0^+\\ \Omega_1^-\end{pmatrix}=\begin{pmatrix}S_{11}&S_{12}\\ S_{21}&S_{22}\end{pmatrix}\begin{pmatrix}\Omega_0^+\\ \Omega_1^-\end{pmatrix}, \tag{10}$$

and using Bloch's theorem, we can derive

$$\begin{pmatrix}S_{11}&0\\ S_{21}&-I\end{pmatrix}\begin{pmatrix}\Omega_0^+\\ \Omega_0^-\end{pmatrix}=e^{i\mathbf{k}\cdot\mathbf{a}_3}\begin{pmatrix}I&-S_{12}\\ 0&-S_{22}\end{pmatrix}\begin{pmatrix}\Omega_0^+\\ \Omega_0^-\end{pmatrix}. \tag{11}$$

Equation (11) is a standard form of generalized eigenproblem $Ax=\lambda Bx$, where *A* and *B* are both square matrices, λ is the eigenvalue, and *x* is the eigenvector. It can be solved by standard eigensolution algorithms such as those provided in the LAPACK libraries. Equation (11) can be written into another form

$$\left[\begin{pmatrix}S_{11}&0\\ S_{21}&-I\end{pmatrix}-e^{i\mathbf{k}\cdot\mathbf{a}_3}\begin{pmatrix}I&-S_{12}\\ 0&-S_{22}\end{pmatrix}\right]\begin{pmatrix}\Omega_0^+\\ \Omega_0^-\end{pmatrix}=P\begin{pmatrix}\Omega_0^+\\ \Omega_0^-\end{pmatrix}=0. \tag{12}$$

Then the eigenproblem is solved by setting $\det(P)=0$, or in another way by finding the zero eigenvalue of the matrix *P*.

Now we have two schemes for solving the same eigenproblem, scheme 1 [Eq. (11)] and scheme 2 [Eq. (12)]. In scheme 2, Bloch's wave vector (k_x, k_y, k_z) is given explicitly as input, the unknown variable is ω. Therefore, it can be classified as $\omega=f(k_x,k_y,k_z)$, similar to the conventional PWM. However, there is a big difference. In the current scheme, the eigenmatrix itself involves the unknown eigenvalue ω. Therefore, the standard eigenproblem solution algorithm is not applicable, instead, one should use other root-searching algorithms of nonlinear equations to find the eigenvalues. There is a merit as compensation for this numerical inconvenience: the current scheme can effectively deal with dispersive materials where ϵ is dispersive with respect to the frequency. Obviously, using this scheme, one can account for the conventional photonic band structures (diagrams plotted along all high-symmetry lines in the first BZ) by only carrying out transfer-matrix calculations along a single stacking direction.

In comparison, scheme 1 can be categorized as $k_z=f(\omega,k_x,k_y)$, with ω and lateral Bloch's wave vector (k_x and k_y) explicitly given as an input, while k_z left to be determined. k_z must be a real number, implying that the eigenvalue $e^{i\mathbf{k}\cdot\mathbf{a}_3}$ must be a complex number of unity modulus. The same concept and principle of this scheme has been widely used in literatures [7,8,11–15], which is called the on-shell approach. In our numerical experiences, the calcu-

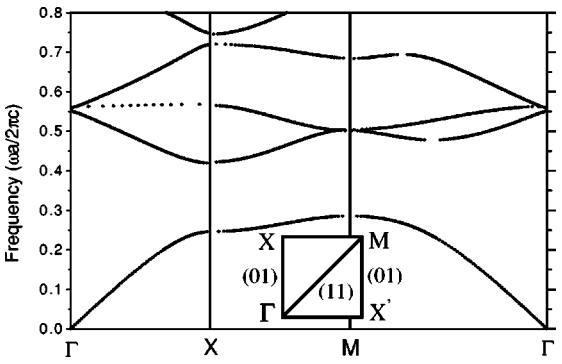

FIG. 2. Diagram of photonic band structures calculated by the plane-wave-based TMM for a 2D square lattice of dielectric cylinders in air under the TM polarization mode. The cylinder has a refractive index of $n=3.4$, and a radius of $r=0.2a$, where a is the lattice constant of the photonic crystal. The inset denotes one quarter of the first BZ of the square lattice.

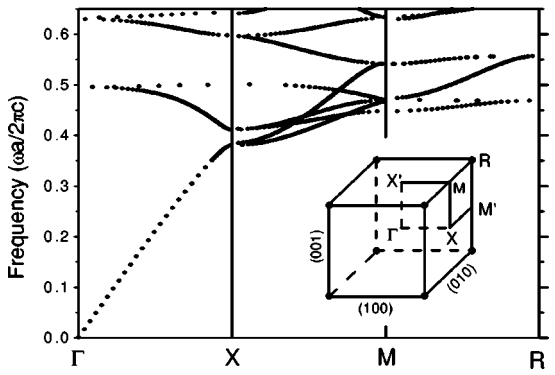

FIG. 3. Diagram of photonic band structures calculated by the plane-wave-based TMM for a 3D simple cubic lattice of dielectric spherical particles embedded in air. The particle has a refractive index of $n=3.4$, and a radius of $r=0.3a$, where a is the lattice constant of the photonic crystal. Inset, first BZ of a simple cubic lattice and corresponding high-symmetry points.

lated eigenvalue corresponding to a Bloch's mode is always of a modulus different from unity within 10^{-10}. Scheme 1 can also apply to dispersive materials. Compared with scheme 2, scheme 1 is most numerically economic to solve the photonic band structure along a prefixed line in the first BZ parallel to the layer stacking direction. In this case, k_x $=$const, $k_y=$const, and $k_z=f(\omega)$. For example, for an fcc lattice, the Γ-X band is solved by considering the (100) stacking direction of the crystal layers, while the Γ-L band should be solved by using the (111) stacking direction. In the following we will use scheme 1 to solve the photonic band structure for 2D photonic crystals composed of dielectric cylinders arrayed in square and triangular lattices, and 3D photonic crystal consisting of cubic lattice of spherical particles. We will use scheme 2 to treat a 3D layer-by-layer photonic crystal arranged in an fct lattice.

III. PHOTONIC BAND STRUCTURES FOR SIMPLE 2D AND 3D LATTICES

The 2D photonic crystal under study is a square lattice of dielectric cylinders in air, where the cylinder has a refractive index of $n=3.4$ and a radius of $r=0.2a$, where a is the lattice constant of the photonic crystal. In the traditional band diagram for a square lattice, the dispersion is calculated along the high-symmetry lines of Γ-X-M-Γ, where Γ $=(0,0)$, $X=(\pi/a,0)$, $M=(\pi/a,\pi/a)$ are high-symmetric points in the first BZ. These three points and corresponding equivalent points are schematically depicted in the inset of Fig. 2, where only one quarter of the first BZ is displayed. Because we prefer to use scheme 1 in Sec. II to solve the photonic band structure, we have set lines Γ-X and X-M in a way that they are both parallel to the (01) crystal direction, because of lattice symmetry. Then, we carry out transfer-matrix calculation along the (01) stacking direction of the cylinder layer. In this direction, the 1D grating has a period of a. The primitive lattice vector is $\mathbf{a}_1=(a,0)$, and another primitive lattice vector along the z axis is $\mathbf{a}_2=(0,a)$. For the Γ-X line, we set $k_x=0$, while for the X-M line, we set k_x $=\pi/a$. The unit-cell thick layer is consisting of two regions, one is the cylinder slab with a thickness of $2r$, the other is an $a-2r$ thick air slab. To calculate the transfer matrix, the cylinder slab is further divided into 10 equal-spacing small slices, each one assumed to be a lamellar grating. The Fourier expansion coefficients of the dielectric function are analytically calculated for each slice. The transfer matrix for the air slab can be analytically derived. For the Γ-M line, we should carry out the transfer-matrix calculation along the (11) crystal direction. In this direction, the 1D grating has a period of $\sqrt{2}a$, with the primitive lattice vector being $\mathbf{a}_1$ $=(\sqrt{2}a,0)$. Another primitive lattice vector along the z-axis direction is $\mathbf{a}_2=(1/2a,\sqrt{2}/2a)$, so there is a phase shift for the transfer matrix. With a layer-to-layer distance of $\sqrt{2}/2a$, the band edge is lying at $k_z=\sqrt{2}(\pi/a)$, which is just the Γ to M distance.

The calculated photonic band structures are displayed in Fig. 2 for the TM (with the electric field parallel to the cylinder axis) polarization mode. A minimum frequency step of $0.0005(2\pi c/a)$ is used in order to account for those flat bands with small dispersion as well as modes close to the band gap edge. Up to 21 plane waves have been used in the transfer-matrix calculations. We have compared with calculations using the conventional PWM for 2D photonic crystals, and found good agreement between the two methods. For instance, the TMM finds a wide TM band gap opening between frequencies $0.2855(2\pi c/a)$ (at the M1 band) and $0.4200(2\pi c/a)$ (at the X2 band), see Fig. 3. Here c is the light speed in vacuum. Calculations by means of the conventional PWM show that this TM band gap is lying between 0.286 and $0.421(2\pi c/a)$. The two results are very close. We have also considered the TE mode, and find that the agreement between the two methods for the TE mode is slightly degraded. We also consider photonic crystals arrayed into a triangular lattice, and find that application of lattice symmetry can also significantly reduce the numerical burden of transfer-matrix calculations.

Now we turn to a more complex structure, a 3D simple cubic lattice of dielectric spheres in air, to see how we can take advantage of the lattice symmetry to calculate the pho-

tonic band structure from as fewer as possible stacking direction of crystal layers. Here we assume that the sphere has a radius of $0.3a$ and a refractive index of 3.4. The first BZ of this crystal and some high-symmetry points are schematically displayed in the inset of Fig. 3. The traditional band diagram is plotted along the high-symmetry lines Γ-X-M-R. Considering the lattice symmetry, we can select three disconnected lines Γ-X', X-M, and M'-R as the equivalent alternative. Since these three lines are all parallel to the (001) direction of the crystal, we can use only one stacking direction of the crystal layers to calculate the whole band diagram. In this direction, the 2D grating is arrayed in a square lattice with primitive lattice vectors $\mathbf{a}_1=(a,0,0)$ and $\mathbf{a}_2=(0,a,0)$, while the third primitive lattice vector along the z axis is $\mathbf{a}_3=(0,0,a)$. For this very simple grating structure, we have carried out the transfer-matrix solution using the scheme of $k_z=f(\omega,k_x,k_y)$ discussed in Sec. III. The photonic band structure using 9×9 plane waves are plotted in Fig. 3. This crystal does not have a complete band gap, as is well known. It does have several directional band gaps along the Γ-X, namely, the (001) or other equivalent directions. If one wishes to further consider the band diagram along the Γ-R line, then one has to consider the (111) stacking direction of the crystal layers. In this plane, the 2D grating is of a 2D triangular lattice with a lattice constant of $\sqrt{2}a$.

IV. PHOTONIC BAND STRUCTURES FOR 3D LAYER-BY-LAYER PHOTONIC CRYSTALS

We proceed further to consider a more complex 3D photonic crystal structure: a layer-by-layer photonic crystal [21,22]. This is an important class of photonic crystal structure that has a complete band gap and has been realized in experiment at the infrared and optical wavelengths. Therefore, it seems justified to carry out a detailed and deliberate examination by means of the new method. The configuration of the photonic crystal is schematically shown in Fig. 4(a). The photonic crystal is formed by stacking rectangular dielectric rods layer by layer consecutively along the (001) direction. Rods in each layer are arrayed into a 1D lamellar grating with a pitch of a. Rods in one layer are perpendicular to those in the next layer, while rods in one layer are shifted by $a/2$ with respect to those in the next two layers. In the (001) plane, the crystal is of a square lattice with a size of a. Each rod is of width w and of thickness h, so that the axis aspect of this crystal is c_0/a, where $c_0=4h$ is the pitch along the (001) direction. The primitive unit cell of the 3D photonic crystal is arrayed into a face-centered tetragonal (fct) lattice. In Fig. 4(a), the coordinate frame (named as XYZ) is selected in a natural way so that the x and y axes are parallel to the two rod extension directions, respectively. The coordinate frame (written as $X'Y'Z'$) for the conventional tetragonal unit cell of an fct lattice is different, in that the x and y axes are of 45° with respect to the rods. Thus, in the (001) plane, the crystal is still of a square lattice, but with a size of $a_0=\sqrt{2}a$. The standard BZ for the fct lattice, as schematically in Fig. 4(b), is also defined in this latter coordinate frame. The coordinate of several high-symmetry points are $\Gamma(0,0,0)$, $X(2\pi/a_0,0,0)$, $T(2\pi/a_0,0,\pi/c_0)$, $L(\pi/a_0,\pi/a_0,\pi/c_0)$, $U(\pi/2a_0,\pi/2a_0,\pi/c_0)$, and $Z(0,0,2\pi/c_0)$. The whole band diagrams should run through these high-symmetry points.

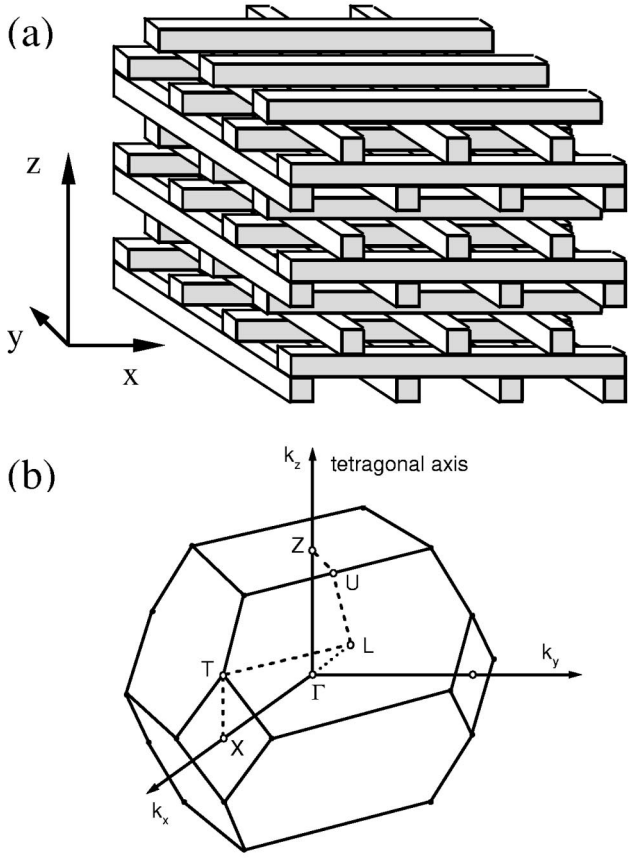

FIG. 4. (a) Schematic configuration of a 3D layer-by-layer photonic crystal composed of rectangular dielectric rods in air. The primitive unit cell is arrayed into an fct lattice. (b) Schematic configuration of the first BZ of a face-centered tetragonal lattice and the corresponding high-symmetry points. Note that the coordinate frames in (a) and (b) are of 45° rotation with respect to each other.

For this complex 3D photonic crystal, if the eigenproblem solution scheme of $k_z=f(\omega,k_x,k_y)$ is used to generate the whole band diagram, several different crystal stacking directions have to be considered separately. In addition, the structural symmetry involved in this layer-by-layer structure is far lower than the fct lattice symmetry itself. This means that we cannot reduce the solution of the whole band diagrams into transfer-matrix calculations along only one or two crystal stacking directions, a way we have done to the simple cubic lattice of spheres. Therefore, we prefer to use the scheme $\omega=f(k_x,k_y,k_z)$. Naturally, the transfer-matrix calculation is performed along the (001) stacking direction of the crystal. In fact, as analyzed in Appendix C, the plane-wave expansion method functions optimally along this direction because of the special geometrical configuration: Each layer is 1D lamellar grating. Usage of deliberately developed Fourier analysis techniques can guarantee fast convergency of the numerical computation. This is another major reason why we

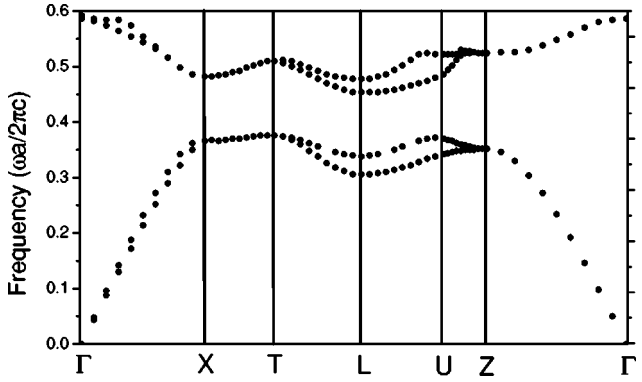

FIG. 5. Diagram of photonic band structures along some high-symmetry lines in the first BZ calculated by the plane-wave-based TMM for a 3D layer-by-layer photonic crystal. The crystal is of a rod-to-rod spacing a, a rod width and thickness of $0.25a$ and $0.3125a$, and a refractive index of the rods $n=3.4$.

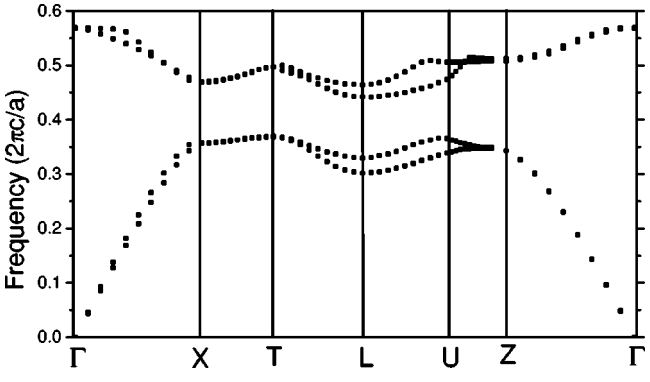

FIG. 6. Diagram of photonic band structures calculated by the conventional PWM for the same 3D layer-by-layer photonic crystal as in Fig. 5.

use the scheme $\omega=f(k_x,k_y,k_z)$ to solve the photonic band structure. Other stacking directions do not possess this merit of superior geometrical configuration.

In the (001) plane, the crystal has a primitive unit cell arrayed into a square lattice with a size of a. The calculation is most convenient in the XYZ coordinate frame, where the two unit vectors are $\mathbf{a}_1=(a,0)$ and $\mathbf{a}_2=(0,a)$, while the third unit vector along the z axis is $\mathbf{a}_3=(a/2,a/2,c_0/2)$, reflecting the fct lattice configuration. The coordinates of the high-symmetry points in this XYZ frame can be obtained by performing a 45° coordinate-rotational transform over those in the $X'Y'Z'$ frame. We write them explicitly here: $\Gamma(0,0,0)$, $X(\pi/a,\pi/a,0)$, $T(\pi/a,\pi/a,\pi/c_0)$, $L(\pi/a,0,\pi/c_0)$, $U(\pi/2a,0,\pi/c_0)$, and $Z(0,0,2\pi/c_0)$. Following the numerical procedures of the eigenproblem scheme $\omega=f(k_x,k_y,k_z)$, for each Bloch's wave vector $\mathbf{k}=(k_x,k_y,k_z)$ within the first BZ, we have been able to determine the eigenfrequency ω that satisfies Eq. (12). Figure 5 displays the lowest 4 photonic bands for a crystal with $w=0.25a$, $h=0.3125a$, and refractive index of the rod as 3.4. The results have been obtained by using a 7×7 plane waves in the transfer-matrix computation. The photonic bands are exactly doubly degenerate along the Γ-Z direction, a natural result is induced by the geometrical symmetry in this direction. There appears a wide complete band gap with the $T2$ band and $L3$ band being the lower and upper band edges, respectively. The band gap is located between frequencies of about $0.376\text{-}0.453(2\pi c/a)$. As a comparison, we have calculated the photonic band structure of the same photonic crystal using the conventional 3D PWM [4–6]. The diagrams of the lowest 4 photonic bands are shown in Fig. 6, where $9\times9\times9$ plane waves have been used. The overall structure of the band diagram in Fig. 6 is similar to that in Fig. 5. However, there are small discrepancy concerning the absolute value of the eigenfrequency. For instance, it is evident that the 3 and 4 bands in Fig. 5 are higher than in Fig. 6, especially along the Γ-Z and Γ-X lines. The same for the complete band gap. In Fig. 6 the complete band gap is lying between 0.370 and $0.442(2\pi c/a)$, about two percents lower than in the TMM.

In order to understand the discrepancy between the two calculations, we have investigated the convergence behavior of the two methods by increasing the plane-wave numbers. The positions of the complete band gap $T2$-$L3$ and the directional band gaps $X2$-$X3$ and $Z2$-$Z3$ are adopted as mirrors to reflect the numerical convergency. The results obtained by the conventional PWM and the plane-wave based TMM are summarized in Tables I and II, respectively. In Table I, the plane-wave number is increased from $5\times5\times5$ to until $13\times13\times13$. In Table II, the plane-wave number is increased from 5×5 to until 11×11. It is quite evident that the former method yields a convergency much slower than the latter method. The latter method has already arrived at an accuracy better than 0.5% with a modest plane-wave number of 7×7. In the former method, all band gaps continue to move to higher frequencies, especially for higher band edge, with a tendency to accord with the converged results given by the latter method. This can explain why in the 3 and 4 bands in Fig. 6 are 2% lower than in Fig. 5. The excellent convergency of the TMM, achieved when applying optimal Fourier expansion rule to the field and dielectric function,

TABLE I. Convergency of the conventional PWM applied to the layer-by-layer photonic crystal.

Plane-wave number	Complete band gap	(001) Band gap	(100) Band gap
$5\times5\times5$	0.3664–0.4343	0.3484–0.5035	0.3539–0.4591
$7\times7\times7$	0.3679–0.4392	0.3483–0.5026	0.3561–0.4663
$9\times9\times9$	0.3696–0.4420	0.3487–0.5078	0.3579–0.4689
$11\times11\times11$	0.3708–0.4439	0.3490–0.5116	0.3592–0.4715
$13\times13\times13$	0.3715–0.4453	0.3491–0.5127	0.3599–0.4729

TABLE II. Convergency of the plane-wave based TMM applied to the layer-by-layer photonic crystal.

Plane-wave number	Complete band gap	(001) Band gap	(100) Band gap
5×5	0.3804–0.4556	0.3543–0.5320	0.3701–0.4824
7×7	0.3762–0.4530	0.3511–0.5247	0.3646–0.4823
9×9	0.3759–0.4522	0.3505–0.5239	0.3645–0.4816
11×11	0.3759–0.4522	0.3504–0.5241	0.3645–0.4813

can set a solid reference to the much more popular conventional PWM. Fairly speaking, the convergency of this popular method is not bad: Using not very large a number of plane-waves, $11\times11\times11$, the predicted width of the complete band gap and other two directional band gaps is only larger than the converged values by less than 1%. Therefore, the wide photonic band gap in this class of layer-by-layer photonic crystal structures is robust irrespective of inaccuracy in previous theoretical methods, and it has been verified by numerous experimental tests. Very recently, the convergence of the conventional PWM applied to another important 3D photonic crystal structure: diamond lattice of dielectric spherical particles in air has been carefully investigated by comparing the PWM result with a convergent KKR calculation [23], and much poorer convergency is found for the PWM [24] compared to the layer-by-layer structure studied here. For instance, the complete band gap size in the close-packed diamond lattice is found to be drastically reduced from the earliest PWM calculation of about 15% [4] to the KKR calculation of 4.2%. Before final conclusion is drawn towards this striking contrast, it might be helpful to employ other independent efficient approach, such as the plane-wave-based TMM presented in this paper, to have a double check.

V. THIRD SCHEME TO SOLVE THE PHOTONIC BAND STRUCTURES

In the above sections we have discussed two different numerical schemes to solve the traditional band diagrams by means of the plane-wave-based TMM. In scheme 1, $k_z = f(k_x, k_y, \omega)$, the transfer matrix is calculated exactly along the stacking direction parallel to the high-symmetry lines in the band diagram. In principle, several stacking directions are needed to account for the whole diagram. In scheme 2, $\omega = f(k_x, k_y, k_z)$, one can calculate the whole diagram of photonic band structures by looking at only one single stacking direction. In scheme 1, very reliable standard eigenproblem solution tools are ready for use, while in scheme 2, consideration of only one stacking direction can reduce the numerical burden. More importantly, it is more flexible to select a stacking direction along which fast converged results can be achieved by using optimal Fourier expansion rules. It may be valuable that one combines the advantages of these two schemes.

Let us take the layer-by-layer photonic crystal as an example. To guarantee fast numerical convergence, we should consider the (001) stacking direction. Now for each $\mathbf{k} = (k_x, k_y, k_z)$, which is usually lying at an arbitrary high-symmetry line, we project it onto the stacking direction, and obtain the lateral wave vector in this plane, which is k_x and k_y. Then we use the scheme $k_z' = f(k_x, k_y, \omega)$ to calculate the dispersion along the (001) direction. Matching k_z' to the prefixed value of k_z either through simple searching or interpolation technique, we can pick up the eigenfrequency corresponding to $\mathbf{k}$, namely, we have arrived at the scheme $\omega = f(k_x, k_y, k_z)$. To speed up the numerical solution, we can first find out the eigenfrequencies at one wave vector, say, the high-symmetry point Z in Fig. 5. Then we start from this point, and carry out the above numerical procedure in the adjacent small frequency range to find out the eigenfrequency of the adjacent wave vector for each photonic band. Repeating this procedure, we can efficiently work out the whole traditional band diagrams.

Similar technique has been used in Refs. [12] and [15], where the overall photonic band structures are investigated by projecting a Bloch's wave vector in traditional first BZ onto the surface Brillouin zone (SBZ) corresponding to the 2D lattice in the lateral XOY plane and then employing the scheme $k_z = f(k_x, k_y, \omega)$ to get the solution. To appreciate the advantage of this scheme, the projection photonic band structures [characterized by $\omega - (k_x, k_y)$] along the high-symmetry lines in the SBZ are plotted, consisting clusters of occupied regions (Bloch's modes) separated by unoccupied regions (directional band gaps). In such forms of band diagrams, only the size of complete band gaps are visible, yet its exact position (upper and lower bands) is invisible (which usually lies at certain high-symmetry points in traditional BZ), so is the size of band gaps along other important crystalline directions. To appreciate these features from direct eye view, traditional band diagrams are preferred, and thus the above simple third scheme can find its usage.

Finally, it seems interesting to compare the current plane-wave based TMM with the more popular real-space TMM [7,8]. Both methods can handle the wave scattering by a finite photonic crystal slab and the photonic band structures for an infinite system. The plane-wave-based method is more flexible in that it can deal with any periodic system with arbitrary lattice types and unit cell configurations. In contrast, the real-space TMM basically is limited to orthogonal lattices due to its use of cubic grid meshes in the finite-difference scheme. Another advantage for the plane-wave-based method is that a lot of advanced analysis tools have been developed in the grating community in the last several decades, in regards to, for example, the convergence problem. As a comparison, in the real-space method, few studies have been reported on such problems, which is essential and important to a numerical method. However, the real-space scheme is superior to the plane-wave-based scheme in one important aspect, that is, it is much faster in constructing the

transfer matrix for a general slab than the plane-wave-based method, because it does not need to solve the eigenproblem for each slice of lamellar grating, which is rather time consuming.

VI. SUMMARY AND CONCLUSION

In summary, we have extended the plane-wave-based TMM from its routine service as a powerful tool to solve em wave scattering by a general multilayer grating and photonic crystal slab to handle the photonic band structure for an infinite system. The numerically stable scattering-matrix algorithm has been used, and three different numerical schemes to solve the eigenproblem corresponding to traditional band diagram have been proposed and discussed in detail. The plane-wave-based TMM allows one to handle arbitrary lattice types and unit-cell configurations. Advanced analysis tools invented in the grating community that allow for efficient Fourier expansion of the dielectric function and em fields with discontinuities occuring at the boundary of different material domains have been exploited to greatly speed up the convergence of numerical computation for 2D and 3D systems. Detailed investigation of the numerical convergence behavior has been carried out for an important class of 3D layer-by-layer photonic crystals by means of both the plane-wave-based TMM and the conventional PWM. The results clearly reveal much better convergency of the TMM.

ACKNOWLEDGMENT

Ames Laboratory is operated for the U.S. Department of Energy (DOE) by Iowa State University under Contract No. W-7405-Eng-82.

APPENDIX A: EIGENMODES WITHIN A 2D LAMELLAR GRATING SLICE AND THE RESULTING TRANSFER MATRIX

In this appendix we will present a detailed description on how the eigenmode of em fields within a 2D lamellar grating slice is solved under the plane-wave basis, and how the transfer-matrix connecting fields at the two hand sides of this grating slice is related to these eigenmodes.

We start from Maxwell's equations,

$$\nabla\times\mathbf{E}(\mathbf{r})=ik_0\mathbf{H}(\mathbf{r}),\quad \nabla\times\mathbf{H}(\mathbf{r})=-ik_0\epsilon(\mathbf{r})\mathbf{E}(\mathbf{r}). \tag{A1}$$

Here $\epsilon(\mathbf{r})$ is the periodic dielectric function of the grating slice, it is homogeneous along the z axis. We can rewrite Eq. (A1) into six partial-differential equations satisfied by (E_x,E_y,E_z) and (H_x,H_y,H_z). The z components of em fields E_z and H_z can be deleted from these six equations, leading to the following four coupled equations:

$$\frac{\partial}{\partial z}E_x=\frac{1}{-ik_0}\frac{\partial}{\partial x}\left[\frac{1}{\epsilon}\left(\frac{\partial}{\partial x}H_y-\frac{\partial}{\partial y}H_x\right)\right]+ik_0H_y, \tag{A2}$$

$$\frac{\partial}{\partial z}E_y=\frac{1}{-ik_0}\frac{\partial}{\partial y}\left[\frac{1}{\epsilon}\left(\frac{\partial}{\partial x}H_y-\frac{\partial}{\partial y}H_x\right)\right]-ik_0H_x, \tag{A3}$$

$$\frac{\partial}{\partial z}H_x=\frac{1}{ik_0}\frac{\partial}{\partial x}\left(\frac{\partial}{\partial x}E_y-\frac{\partial}{\partial y}E_x\right)-ik_0\epsilon E_y, \tag{A4}$$

$$\frac{\partial}{\partial z}H_y=\frac{1}{ik_0}\frac{\partial}{\partial y}\left(\frac{\partial}{\partial x}E_y-\frac{\partial}{\partial y}E_x\right)+ik_0\epsilon E_x. \tag{A5}$$

We can further write down the plane-wave expansion expressions of the em fields [already given in Eqs. (1) and (2)] and the dielectric function,

$$\epsilon(\mathbf{r})=\sum_{ij}\ \epsilon_{ij}e^{i\mathbf{G}_{ij}\cdot\mathbf{r}}, \tag{A6}$$

$$\epsilon^{-1}(\mathbf{r})=\sum_{ij}\ \epsilon_{ij}^{-1}e^{i\mathbf{G}_{ij}\cdot\mathbf{r}}. \tag{A7}$$

Substituting them into Eqs. (A2)–(A5) yields

$$\frac{\partial}{\partial z}E_{ij,x}=\frac{-ik_{ij,x}}{k_0}\sum_{mn}\ \epsilon^{-1}_{ij;mn}(k_{mn,x}H_{mn,y}-k_{mn,y}H_{mn,x})+ik_0H_{ij,y}, \tag{A8}$$

$$\frac{\partial}{\partial z}E_{ij,y}=\frac{-ik_{ij,y}}{k_0}\sum_{mn}\ \epsilon^{-1}_{ij;mn}(k_{mn,x}H_{mn,y}-k_{mn,y}H_{mn,x})-ik_0H_{ij,x}, \tag{A9}$$

$$\frac{\partial}{\partial z}H_{ij,x}=\frac{ik_{ij,x}}{k_0}\sum_{mn}\ \delta_{ij;mn}(k_{mn,x}E_{mn,y}-k_{mn,y}E_{mn,x})-ik_0\sum_{mn}\ \epsilon_{ij;mn}E_{mn,y}, \tag{A10}$$

$$\frac{\partial}{\partial z}H_{ij,y}=\frac{ik_{ij,x}}{k_0}\sum_{mn}\ \delta_{ij;mn}(k_{mn,x}E_{mn,y}-k_{mn,y}E_{mn,x})+ik_0\sum_{mn}\ \epsilon_{ij;mn}E_{mn,x}. \tag{A11}$$

Now define column vectors $E=(\cdots,E_{ij,x},E_{ij,y},\cdots)^T$ and $H=(\cdots,H_{ij,x},H_{ij,y},\cdots)^T$, Eqs. (A8)–(A11) can be written into a concise matrix form

$$\frac{\partial}{\partial z}E=T_1H,\quad \frac{\partial}{\partial z}H=T_2E, \tag{A12}$$

where the matrices T_1 and T_2 are defined as

$$T_1^{ij;mn}=\frac{i}{k_0}\begin{pmatrix} k_{ij,x}\epsilon^{-1}_{ij;mn}k_{mn,y} & -k_{ij,x}\epsilon^{-1}_{ij;mn}k_{mn,x}+k_0^2\delta_{ij;mn} \\ k_{ij,y}\epsilon^{-1}_{ij;mn}k_{mn,y}-k_0^2\delta_{ij;mn} & -k_{ij,y}\epsilon^{-1}_{ij;mn}k_{mn,x}\end{pmatrix},$$

$$T_2^{ij;mn}=\frac{i}{k_0}\begin{pmatrix} -k_{ij,x}\delta_{ij;mn}k_{mn,y} & k_{ij,x}\delta_{ij;mn}k_{mn,x}-k_0^2\epsilon_{ij;mn} \\ -k_{ij,y}\delta_{ij;mn}k_{mn,y}+k_0^2\epsilon_{ij;mn} & k_{ij,y}\delta_{ij;mn}k_{mn,x}\end{pmatrix}.$$

From Eq. (A12) we finally obtain an eigenproblem for the electric field,

$$\frac{\partial^2}{\partial z^2}E=(T_1T_2)E=PE. \tag{A13}$$

Now suppose we have used N_0 plane waves in the expansion, then T_1, T_2, and P are all $(2N_0)\times(2N_0)$ matrices. Solution of Eq. (A13) will give us $2N_0$ eigenvalues (denoted as $\beta_i^2, i=1,2,\ldots,2N_0$, with $\mathrm{Im}(\beta_i)\geqslant 0$) of the matrix $-P=-T_1T_2$. In addition, the $(2N_0)\times(2N_0)$ matrix S_a, whose jth column is the eigenvector corresponding to the eigenvalue β_j^2, can also be obtained simultaneously. The eigenmode corresponding to β_i^2 is $E_i'(z)=E_{a,i}^+(z)+E_{a,i}^-(z)$, $E_{a,i}^+(z)=E_i^+e^{i\beta_i(z-z_{i-1})}$, $E_{a,i}^-(z)=E_i^-e^{-i\beta_i(z-z_{i-1})}$, where E_i^+ and E_i^- are both unknown variables. Further define column vector $\beta=(\ldots,\beta_i,\ldots)^T$, $E_a^+=[\ldots,E_{a,i}^+(z),\ldots]^T$, and $E_a^-=[\ldots,E_{a,i}^-(z),\ldots]^T$. The electric field column vector E are now expressed into the superposition of all the eigenmodes, $E=S_a(E_a^++E_a^-)$. The corresponding magnetic field column vector are obtained from Eq. (A12) and reads $H=T_1^{-1}\partial/\partial zE=T_1^{-1}S_a\partial/\partial z(E_a^++E_a^-)=iT_1^{-1}S_a\beta(E_a^+-E_a^-)=T_a(E_a^+-E_a^-)$, where $T_a=iT_1^{-1}S_a\beta$. It proves convenient to write down the electric and magnetic fields at an arbitrary point inside the grating slice into a concise form:

$$\begin{pmatrix}E(z)\\H(z)\end{pmatrix}=\begin{pmatrix}S_a & S_a\\ T_a & -T_a\end{pmatrix}\begin{pmatrix}E_a^+(z)\\E_a^-(z)\end{pmatrix}. \tag{A14}$$

The em fields in the two air films around the grating slice have been expressed in Eqs. (3) and (4), and can be rewritten in a way similar to Eq. (A14). Match of boundary conditions yields

$$\begin{pmatrix}S_0 & S_0\\ T_0 & -T_0\end{pmatrix}\begin{pmatrix}\Omega_{i-1}^+\\ \Omega_{i-1}^-\end{pmatrix}=\begin{pmatrix}S_a & S_a\\ T_a & -T_a\end{pmatrix}\begin{pmatrix}E_a^+(z_{i-1})\\ E_a^-(z_{i-1})\end{pmatrix} \tag{A15}$$

at the left interface $z=z_{i-1}$ and

$$\begin{pmatrix}S_0 & S_0\\ T_0 & -T_0\end{pmatrix}\begin{pmatrix}\Omega_{i}^+\\ \Omega_{i}^-\end{pmatrix}=\begin{pmatrix}S_a & S_a\\ T_a & -T_a\end{pmatrix}\begin{pmatrix}E_a^+(z_{i})\\ E_a^-(z_{i})\end{pmatrix} \tag{A16}$$

at the right interface $z=z_i$. S_0 and T_0 are counterparts of S_a and T_a in an air film. $S_0=I$, a unit matrix, and T_0 is a block-diagonal matrix each block of which is a 2×2 matrix already given by $T_{0,ij}$ in Eq. (4). Within the grating slice,

$$\begin{pmatrix}E_a^+(z_i)\\E_a^-(z_i)\end{pmatrix}=\begin{pmatrix}e^{i\beta h} & 0\\ 0 & e^{-i\beta h}\end{pmatrix}\begin{pmatrix}E_a^+(z_{i-1})\\E_a^-(z_{i-1})\end{pmatrix}, \tag{A17}$$

where $h=z_i-z_{i-1}$ is the thickness of the slice, $e^{i\beta h}$ denotes a $(2N_0)\times(2N_0)$ diagonal matrix whose element is $e^{i\beta_i h}$, $i=1,2,\ldots,2N_0$. Deleting $[E_a^+(z_{i-1}),E_a^-(z_{i-1})]^T$ and $[E_a^+(z_i),E_a^-(z_i)]^T$ from Eqs. (A15)–(A17) and making some analytical derivations yields

$$\begin{pmatrix}\Omega_i^+\\ \Omega_i^-\end{pmatrix}=\begin{pmatrix}a_{11} & a_{12}\\ a_{21} & a_{22}\end{pmatrix}^{-1}\begin{pmatrix}e^{i\beta h} & 0\\ 0 & e^{-i\beta h}\end{pmatrix}\begin{pmatrix}a_{11} & a_{12}\\ a_{21} & a_{22}\end{pmatrix}\begin{pmatrix}\Omega_{i-1}^+\\ \Omega_{i-1}^-\end{pmatrix}, \tag{A18}$$

where $a_{11}=\frac{1}{2}(S_a^{-1}S_0+T_a^{-1}T_0)$, $a_{12}=\frac{1}{2}(S_a^{-1}S_0-T_a^{-1}T_0)$, and $a_{21}=a_{12}$, $a_{22}=a_{11}$. Thus the T matrix for slice i is

$$T_i=\begin{pmatrix}t_{11}^i & t_{12}^i\\ t_{21}^i & t_{22}^i\end{pmatrix}=\begin{pmatrix}a_{11} & a_{12}\\ a_{21} & a_{22}\end{pmatrix}^{-1}\begin{pmatrix}e^{i\beta h} & 0\\ 0 & e^{-i\beta h}\end{pmatrix}\begin{pmatrix}a_{11} & a_{12}\\ a_{21} & a_{22}\end{pmatrix}. \tag{A19}$$

Now it becomes clear why the T-matrix formalism is numerically unstable for thick gratings. Look at the two phase factors $e^{i\beta h}$ and $e^{-i\beta h}$. For those Bragg wave components where β_i has a significant imaginary part, one of them must be exponentially increasing through the whole slab of gratings, rendering numerical instability such as overflow.

In principle, the S matrix can be calculated from the T matrix through transformation: $s_{11}^i=t_{11}^i-t_{12}^i[t_{22}^i]^{-1}t_{21}^i$, $s_{12}^i=t_{12}^i[t_{22}^i]^{-1}$, $s_{21}^i=-[t_{22}^i]^{-1}t_{21}^i$, $s_{22}^i=[t_{22}^i]^{-1}$. However, because the T-matrix algorithm is not stable, we prefer to derive the S matrix for slice i directly from Eq. (A18) without the aid of the T matrix, largely depending on analytical derivation. The final answer is

$$s^i=\begin{pmatrix}s_{11}^i & s_{12}^i\\ s_{21}^i & s_{22}^i\end{pmatrix}=\begin{pmatrix}p_1t_1+p_2t_2 & p_1t_2+p_2t_1\\ p_1t_2+p_2t_1 & p_1t_1+p_2t_2\end{pmatrix}, \tag{A20}$$

where $p_1=[a_{11}-e^{i\beta h}a_{12}a_{11}^{-1}e^{i\beta h}a_{12}]^{-1}$, $p_2=a_{11}^{-1}e^{i\beta h}a_{12}[a_{11}-e^{i\beta h}a_{12}a_{11}^{-1}e^{i\beta h}a_{12}]^{-1}$, $t_1=e^{i\beta h}a_{11}$, and $t_2=-a_{12}$. From Eq. (A20), it is obvious that s^i is a block-

symmetric matrix, reflecting the fact that the grating slice is symmetric with respect to its middle plane at $z=(z_{i-1}+z_i)/2$.

APPENDIX B: EIGENMODES WITHIN A 1D LAMELLAR GRATING SLICE

In this appendix we will derive the eigenmode of em fields within a 1D lamellar grating slice directly from the general 2D case. Both the TM and TE polarization modes will be considered simultaneously.

In recent years, powerful analytical tools of Fourier expansion for the dielectric function and em fields applied to a 1D grating have been developed. The optimal Fourier expansion rule can efficiently handle the subtle discontinuity of ϵ and em fields at the boundary of the two different material domains, and allows for accelerated numerical convergency [18,19]. These rules can be summarized as follows. Consider $D=\epsilon E$, where D and E are one of the three components of the electric displacement and electric field vectors, if E is continuous across the boundary, then the direct Fourier transformation over ϵ should be used to Fourier transform D, namely, $D_i=\epsilon_{ij}E_j$. Here doubly appearance of the index "j" means summation over "j". If D is continuous across the boundary, then the inverse rule of Fourier expansion over ϵ should be used, $D_i=[(1/\epsilon)]^{-1}_{ij}E_j$, where $[(1/\epsilon)]^{-1}$ means the inverse matrix of the Fourier transformation matrix of the function $1/\epsilon$.

Now suppose a 1D lamellar grating is periodic along the y axis and homogeneous along the x axis. For the TM mode, the field variables are (E_x,H_y), while for the TE mode, the field variables are (E_y,H_x). Following the above rules and using Eqs. (A12) and(A13), the optimal form of the eigenproblem for the TM mode is

$$\frac{\partial^2}{\partial z^2}E_x=(T_1T_2)E_x=PE_x, \tag{B1}$$

where $T_1^{j;n}=ik_0\delta_{j;n}$, $T_2^{j;n}=(i/k_0)(-k_{j,y}^2+k_0^2\epsilon_{j;n})$. For the TE mode, we have

$$\frac{\partial^2}{\partial z^2}E_y=(T_1T_2)E_y=PE_y, \tag{B2}$$

where $T_1^{j;n}=(i/k_0)(k_{j,y}\epsilon_{j;n}^{-1}k_{n,y}-k_0^2\delta_{j;n})$, $T_2^{j;n}=-ik_0[(1/\epsilon)]^{-1}_{j;n}$. In the above, $\epsilon_{j;n}$ is the direct Fourier expansion coefficient of $\epsilon(y)$. $\epsilon^{-1}_{j;n}$ is obtained by the inverse matrix of $\epsilon_{j;n}$, following from $D_z=\epsilon E_z$ in Eqs. (A1)–(A3), where E_z is always continuous at the boundary, since it is parallel to the domain wall of lamellar gratings. $[(1/\epsilon(y))]^{-1}_{j;n}$ is obtained by first Fourier transform over $1/\epsilon(y)$, then inverse the resulting matrix.

When the eigenmode within the 1D lamellar grating have been solved via Eqs. (B1) and (B2), the corresponding transfer matrix, either the T matrix or S matrix, can be obtained following the same procedure for the general 2D case discussed in Appendix A.

APPENDIX C: OPTIMAL FOURIER EXPANSION RULE FOR A LAYER-BY-LAYER PHOTONIC CRYSTAL

In this appendix we will present the optimal Fourier expansion rule for an important class of 3D photonic crystal: layer-by-layer photonic crystals. This can be done because of the special geometrical configuration of this kind of photonic crystal, where each layer of rectangular rods in air is a 1D lamellar grating, so that the effective and efficient rule developed in Appendix B can be directly utilized. The rapid convergence behavior of numerical calculations allow us to use this as a reference to appraise the convergency of the conventional PWM when applied to this important 3D photonic crystal structure.

In Appendix A, we have not used the optimal Fourier expansion rule for the discontinuous dielectric functions $\epsilon(\mathbf{r})$ and $\epsilon^{-1}(\mathbf{r})$ in a 3D photonic crystal. Now following the rules described in Appendix B, for a layer where the rods are along the x-axis direction, T_1 and T_2 in Eq. (A12) should be written as

$$T_1^{ij;mn}=\frac{i}{k_0}\begin{pmatrix} k_{ij,x}\epsilon^{-1}_{ij;mn}k_{mn,y} & -k_{ij,x}\epsilon^{-1}_{ij;mn}k_{mn,x}+k_0^2\delta_{ij;mn} \\ k_{ij,y}\epsilon^{-1}_{ij;mn}k_{mn,y}-k_0^2\delta_{ij;mn} & -k_{ij,y}\epsilon^{-1}_{ij;mn}k_{mn,x}\end{pmatrix},$$

$$T_2^{ij;mn}=\frac{i}{k_0}\begin{pmatrix} -k_{ij,x}\delta_{ij;mn}k_{mn,y} & k_{ij,x}\delta_{ij;mn}k_{mn,x}-k_0^2\left[\left(\frac{1}{\epsilon}\right)\right]^{-1}_{ij;mn} \\ -k_{ij,y}\delta_{ij;mn}k_{mn,y}+k_0^2\epsilon_{ij;mn} & k_{ij,y}\delta_{ij;mn}k_{mn,x}\end{pmatrix}.$$

The reason is that E_x and E_z are both parallel to the air-rod boundary, while E_y is perpendicular to the air-rod boundary. For the same reason, for a layer where the rods are along the y-axis direction, T_1 and T_2 in Eq. (A12) should be

$$T_1^{ij;mn}=\frac{i}{k_0}\begin{pmatrix} k_{ij,x}\epsilon^{-1}_{ij;mn}k_{mn,y} & -k_{ij,x}\epsilon^{-1}_{ij;mn}k_{mn,x}+k_0^2\delta_{ij;mn} \\ k_{ij,y}\epsilon^{-1}_{ij;mn}k_{mn,y}-k_0^2\delta_{ij;mn} & -k_{ij,y}\epsilon^{-1}_{ij;mn}k_{mn,x}\end{pmatrix},$$

$$T_2^{ij;mn} = \frac{i}{k_0} \begin{pmatrix} -k_{ij,x}\delta_{ij;mn}k_{mn,y} & k_{ij,x}\delta_{ij;mn}k_{mn,x} - k_0^2\epsilon_{ij;mn} \\ -k_{ij,y}\delta_{ij;mn}k_{mn,y} + k_0^2\left[\left(\frac{1}{\epsilon}\right)\right]^{-1}_{ij;mn} & k_{ij,y}\delta_{ij;mn}k_{mn,x} \end{pmatrix}.$$

It should be noted that until now, optimal Fourier expansion rules as powerful as the above for 1D gratings are still to be found for a general 3D photonic crystal with arbitrary geometrical configuration, although promising progress has been made [18,19]. For a 3D photonic crystal built from spherical particles, such as the simple cubic lattice considered in Sec. III, we simply use the direct rule of Fourier expansion rule for $\epsilon_{ij;mn}$, and inverse rule for $\epsilon^{-1}_{ij;mn}$ in the matrices T_1 and T_2 in (A12) of Appendix A.

[1] E. Yablonovitch, Phys. Rev. Lett. **58**, 2059 (1987).
[2] J.D. Joannopoulos, P.R. Villeneuve, and S. Fan, Nature (London) **386**, 143 (1997).
[3] K. Sakoda, *Optical Properties of Photonic Crystals* (Springer, Berlin, 2001).
[4] K.M. Ho, C.T. Chan, and C.M. Soukoulis, Phys. Rev. Lett. **65**, 3152 (1990).
[5] D. Cassagne, C. Jouanin, and D. Bertho, Phys. Rev. B **53**, 7134 (1996).
[6] Z.Y. Li, J. Wang, and B.Y. Gu, Phys. Rev. B **58**, 3721 (1998).
[7] J.B. Pendry, J. Mod. Opt. **41**, 209 (1994).
[8] P.M. Bell, J.B. Pendry, L. Marin Moreno, and A.J. Ward, Comput. Phys. Commun. **85**, 306 (1995).
[9] C.T. Chan, Q.L. Yu, and K.M. Ho, Phys. Rev. B **51**, 16 635 (1995).
[10] N.A. Nicorovici, R.C. McPhedran, and L.C. Botten, Phys. Rev. E **52**, 1135 (1995).
[11] N. Stefanou, V. Yannopapas, and A. Modinos, Comput. Phys. Commun. **113**, 49 (1998).
[12] A. Modinos, N. Stefanou, and V. Yannopapas, Opt. Express **8**, 197 (2001).
[13] W. Zhang, C.T. Chan, and P. Sheng, Opt. Express **8**, 203 (2001).
[14] L.C. Botten, N.A. Nicorovici, R.C. McPhedran, C. Martijn de Sterke, and A.A. Asatryan, Phys. Rev. E **64**, 046603 (2001).
[15] B. Gralak, S. Enoch, and G. Tayeb, J. Opt. Soc. Am. A **19**, 1547 (2002).
[16] M.G. Moharam and T.K. Gaylord, J. Opt. Soc. Am. **72**, 1385 (1982).
[17] M.G. Moharam, E.B. Grann, D.A. Pommet, and T.K. Gaylord, J. Opt. Soc. Am. A **12**, 1068 (1995).
[18] L. Li, J. Opt. Soc. Am. A **13**, 1870 (1996).
[19] L. Li, J. Opt. Soc. Am. A **14**, 2758 (1997).
[20] L. Li, J. Opt. Soc. Am. A **13**, 1024 (1996).
[21] K.M. Ho, C.T. Chan, C.M. Soukoulis, R. Biswas, and M. Sigalas, Solid State Commun. **89**, 413 (1994).
[22] S.Y. Lin, J.G. Fleming, D.L. Hetherington, B.K. Smith, R. Biswas, K.M. Ho, M.M. Sigalas, W. Zurbrzycki, S.R. Kurtz, and J. Bur, Nature (London) **394**, 251 (1998).
[23] A. Moroz, Phys. Rev. B **66**, 115109 (2002).
[24] S.G. Johnson and J.D. Joannopoulos, Opt. Express **8**, 173 (2001).